RSC Advances

ROYAL SOCIETY OF CHEMISTRY

www.rsc.org/advances

Exploring 5-fluoronicotinic acid as a versatile building block for the generation of topologically diverse metal-organic and supramolecular Ni, Co, and Cd networks

Yan-Hui Cui,[a] Jiang Wu,[a] Alexander M. Kirillov,[b] Jin-Zhong Gu*[a] and Wei Dou[a]

[a] *Key Laboratory of Nonferrous Metal Chemistry and Resources Utilization of Gansu Province, College of Chemistry and Chemical Engineering, Lanzhou University, Lanzhou 730000, P. R. China*

[b] *Centro de Química Estrutural, Complexo I, Instituto Superior Técnico, Universidade de Lisboa, Av. Rovisco Pais, 1049-001, Lisbon, Portugal*

* Corresponding author. Fax: +86 931 8915196. *E-mail address*: gujzh@lzu.edu.cn (J.-Z. Gu).

Abstract

Five new coordination compounds, namely $[Ni(5\text{-Fnic})_2(\mu_2\text{-}H_2O)_{0.5}]_n$ (**1**), $[Co(5\text{-Fnic})_2(H_2biim)]_n$ (**2**), $\{[Cd(5\text{-Fnic})_2(phen)]\cdot 2H_2O\}_n$ (**3**), $[Cd(5\text{-Fnic})_2(H_2biim)_2]$ (**4**), and $[Co(5\text{-Fnic})_2(H_2O)_4]$ (**5**), were generated by hydrothermal method from the metal(II) nitrates, 5-fluoronicotinic acid (5-FnicH), and an optional ancillary 1,10-phenanthroline (phen) or 2,2′-biimidazole (H_2biim) ligand. All the products **1**–**5** were characterized by IR spectroscopy, elemental, thermogravimetric, and single-crystal X-ray diffraction analyses. Their structures range from the intricate 3D metal-organic framework (MOF) **1** to the 1D coordination polymers **2** and **3**, and the discrete 0D monomers **4** and **5**. The structures of **2**–**5** are further extended [1D→2D (**2**), 1D→1D (**3**), 0D→1D (**4**), and 0D→3D (**5**)] into various H-bonded networks. The topological analysis of the underlying coordination (in **1**) and H-bonded (in **2**–**5**) nets revealed a very rare **3,6T10** MOF topology in **1**, a parallel 2D+2D interpenetration of the **sql** nets in **2**, a topologically unique double chain in **3**, a simple **2C1** topology in **4**, and a **pcu** (alpha-Po primitive cubic) topology in **5**. The magnetic (for **1** and **2**) and luminescent (for **3** and **4**) properties were also investigated and discussed.

Keywords: 5-Fluoronicotinic acid, coordination polymers, photoluminescence, magnetism, crystal engineering.

1. Introduction

The design and synthesis of coordination polymers, metal-organic frameworks and discrete complexes have been of considerable interest owing to their diversity of intriguing coordination and supramolecular architectures and topological features, as well as various applications in different areas.[1–6] Aromatic carboxylate ligands are recognized building blocks in the construction of compounds with high-dimensional networks and interesting properties, not only due to their ability of adapting diverse coordination modes and showing high stability, but also because of potential function as H-bond donors and acceptors.[7–13] In many cases, the synthesis of coordination compounds is based on self-assembly methods that are highly influenced by a number of factors, including the nature of metal ions and ligands, type of reaction medium, presence of templates and ancillary ligands, stoichiometry and various reaction conditions.[8,9,11] Apart from carboxylate ligands, 1,10-phenanthroline (phen) and 2,2′-biimidazole (H_2biim) have often been used as secondary N,N-donor building blocks to construct and stabilize new structures, on account of their effective π···π stacking and/or weak H-bonding interactions.[8,9,12,14]

As a continuation of our research in this field,[8,9,12] we have tested the hydrothermal self-assembly reactions of various metal(II) nitrates (M = Cd, Co, Ni) with 5-fluoronicotinic acid (5-FnicH) as a main building block and 1,10-phenanthroline (phen) or 2,2′-biimidazole (H_2biim) as N,N-donor ancillary ligands in view of the following considerations. (A) 5-Fluoronicotinic acid remains very scarcely explored in the crystal engineering of coordination polymers, as attested by a search of Cambridge Crystallographic Database (CSD) that revealed only four structurally

characterized coordination compounds derived from this acid.[15] (B) 5-FnicH possesses one carboxylic group and one pyridyl N atom available for coordination to a metal center, while the presence of tethered fluoride functionality affects its acidity in comparison with unsubstituted nicotinic acid, thus potentially allowing the formation of structurally different coordination compounds. (C) The introduction of phen and H_2biim ligands may facilitate the crystallization of compounds and stabilization of their structures.

Hence, by employing 5-FnicH as a main building block and introducing an optional ancillary N,N-donor ligand, we have produced by hydrothermal self-assembly method a series of novel coordination compounds, namely a 3D metal-organic framework $[Ni(5\text{-Fnic})_2(\mu_2\text{-}H_2O)_{0.5}]_n$ (**1**), 1D coordination polymers $[Co(5\text{-Fnic})_2(H_2biim)]_n$ (**2**) and $\{[Cd(5\text{-Fnic})_2(phen)]\cdot 2H_2O\}_n$ (**3**), and discrete 0D complexes $[Cd(5\text{-Fnic})_2(H_2biim)_2]$ (**4**) and $[Co(5\text{-Fnic})_2(H_2O)_4]$ (**5**). Their diversity indicates that the type of metal ion and ancillary ligand have an important effect on the formation, structural and topological features of the final products **1**–**5**. All the compounds were characterized by IR spectroscopy, elemental, thermogravimetric, and single-crystal X-ray diffraction analyses. The magnetic behavior of **1** and **2** and the luminescent properties of **3** and **4** were also studied.

2. Experimental

2.1 Materials and methods

All chemicals and solvents were of A.R. grade and used without further purification.

Carbon, hydrogen, and nitrogen content in **1**–**5** was determined using an Elementar Vario EL elemental analyzer. IR spectra were recorded in KBr pellets and a Bruker EQUINOX 55 spectrometer. Thermogravimetric analysis (TGA) was performed under N_2 atmosphere with a heating rate of 10 °C/min on a LINSEIS STA PT1600 thermal analyzer. Magnetic susceptibility data were collected in the 2–300 K temperature range with a Quantum Design SQUID Magnetometer MPMS XL-7 with a field of 0.1 T. A correction was made for the diamagnetic contribution prior to data analysis. Excitation and emission spectra were recorded for the solid samples on an Edinburgh FLS920 fluorescence spectrometer at room temperature.

2.2 Synthesis of $[Ni(5\text{-}Fnic)_2(\mu_2\text{-}H_2O)_{0.5}]_n$ (1)

A mixture of $Ni(NO_3)_2{\cdot}6H_2O$ (43.6 mg, 0.15 mmol), 5-FnicH (42.3 mg, 0.3 mmol), NaOH (12.0 mg, 0.3 mmol), and H_2O (10 mL) was stirred at room temperature for 15 min, then sealed in a 25 mL Teflon-lined stainless steel vessel, and heated at 160 ℃ for 3 days, followed by cooling to room temperature at a rate of 10 °C/h. Green needle-shaped crystals were isolated manually, washed with distilled water and dried to give **1**. Yield: 65% (based on 5-FnicH). Calcd for $C_{12}H_7F_2NiN_2O_{4.5}$: C 41.43, H 2.03, N 8.05%. Found: C 41.78, H 2.13, N 8.41%. IR (KBr, cm^{-1}): 3286m, 3067w, 1618m, 1593s, 1457w, 1388s, 1300m, 1256m, 1161w, 1141w, 1029w, 954w, 922w, 800s, 691m, 566w , 458w.

2.3 Synthesis of $[Co(5\text{-}Fnic)_2(H_2biim)]_n$ (2)

A mixture of $Co(NO_3)_2 \cdot 6H_2O$ (43.6 mg, 0.15 mmol), 5-FnicH (42.3 mg, 0.3 mmol), H_2biim (20.1 mg, 0.15 mmol), NaOH (12.0 mg, 0.3 mmol), and H_2O (10 mL) was stirred at room temperature for 15 min, then sealed in a 25 mL Teflon-lined stainless steel vessel, and heated at 160 °C for 3 days, followed by cooling to room temperature at a rate of 10 °C/h. Pink needle-shaped crystals were isolated manually, washed with distilled water and dried to furnish **2**. Yield: 60% (based on 5-FnicH). Calcd for $C_{18}H_{12}F_2CoN_6O_4$: C 45.68, H 2.56, N 17.76%. Found: C 45.29, H 2.65, N 17.37%. IR (KBr, cm^{-1}): 1615s, 1573s, 1461w, 1402s, 1382vs, 1334w, 1287w, 1245w, 1153w, 1125m, 1030w, 990m, 959w, 946w, 924w, 907w, 854w, 819m, 796m, 783m, 768w, 752m, 694m, 574w, 429m.

2.4 Synthesis of $\{[Cd(5\text{-}Fnic)_2(phen)]\cdot 2H_2O\}_n$ (3)

A mixture of $Cd(NO_3)_2 \cdot 4H_2O$ (46.2 mg, 0.15 mmol), 5-FnicH (42.3 mg, 0.3 mmol), phen (30.0 mg, 0.15 mmol), NaOH (12.0 mg, 0.3 mmol), and H_2O (10 mL) was stirred at room temperature for 15 min, then sealed in a 25 mL Teflon-lined stainless steel vessel, and heated at 160 °C for 3 days, followed by cooling to room temperature at a rate of 10 °C/h. Colorless block-shaped crystals were isolated manually, washed with distilled water and dried to produce **3**. Yield: 60% (based on 5-FnicH). Calcd for $C_{24}H_{18}F_2CdN_4O_6$: C 47.35, H 2.98, N 9.20%. Found: C 47.72, H 3.12, N 8.89%. IR (KBr, cm^{-1}): 3437m, 3055m, 1611s, 1569s, 1516m, 1459m, 1427w, 1399s, 1293m, 1240m, 1155m, 1139w, 1102w, 1026w, 948w, 916w, 849m, 790s, 727m, 693m, 638w, 565w, 425w.

2.5 Synthesis of [Cd(5-Fnic)$_2$(H$_2$biim)$_2$] (4)

A mixture of $Cd(NO_3)_2 \cdot 4H_2O$ (46.2 mg, 0.15 mmol), 5-FnicH (42.3 mg, 0.3 mmol), H_2biim (40.2 mg, 0.30 mmol), NaOH (12.0 mg, 0.3 mmol), and H_2O (10 mL) was stirred at room temperature for 15 min, then sealed in a 25 mL Teflon-lined stainless steel vessel, and heated at 160 °C for 3 days, followed by cooling to room temperature at a rate of 10 °C/h. Yellow block-shaped crystals were isolated manually, washed with distilled water and dried to give **4**. Yield: 55% (based on 5-FnicH). Calcd for $C_{24}H_{18}F_2CdN_{10}O_4$: C 43.62, H 2.74, N 21.19%. Found: C 43.26, H 2.86, N 20.83. IR (KBr, cm^{-1}): 1593s, 1562s, 1455m, 1425m, 1373vs, 1331w, 1240m, 1181w, 1148w, 1133w, 1122w, 1099w, 1025w, 995m, 946m, 892m, 859w, 782s, 760m, 691s, 661w, 580w, 529w, 491w, 431w, 405w.

2.6 Synthesis of [Co(5-Fnic)$_2$(H$_2$O)$_4$] (5)

A mixture of $Co(NO_3)_2 \cdot 6H_2O$ (43.6 mg, 0.15 mmol), 5-FnicH (42.3 mg, 0.3 mmol), NaOH (12.0 mg, 0.3 mmol), and H_2O (10 mL) was stirred at room temperature for 15 min, then sealed in a 25 mL Teflon-lined stainless steel vessel, and heated at 160 °C for 3 days, followed by cooling to room temperature at a rate of 10 °C/h. Pink needle-shaped crystals were isolated manually, washed with distilled water and dried to produce **5**. Yield: 60% (based on 5-FnicH). Calcd for $C_{12}H_{14}F_2CoN_2O_8$: C 35.05, H 3.43, N 6.81%. Found: C 34.71, H 3.58, N 7.13%. IR (KBr, cm^{-1}): 3285s, 1617s, 1593s, 1457m, 1386s, 1300s, 1255m, 1159w, 1139w, 1028w, 952w, 921m, 799m,

690w, 564w, 458w.

3. X-ray crystallography

The single-crystal X-ray data collection for **1**–**5** was performed on a Bruker Smart CCD diffractometer, using graphite-monochromated Mo K_α radiation (λ = 0.71073 Å). Semiempirical absorption corrections were applied using the SADABS program. The structures were solved by direct methods and refined by full-matrix least-squares on F^2 with the SHELXS-97 and SHELXL-97 programs.[16] All the non-hydrogen atoms were refined anisotropically by full-matrix least-squares methods on F^2. All the hydrogen atoms (except those bound to water molecules) were placed in calculated positions with fixed isotropic thermal parameters and included in structure factor calculations at the final stage of full-matrix least-squares refinement. The hydrogen atoms of water molecules were located by difference maps and constrained to ride on their parent O atoms. The crystal data for **1**–**5** are summarized in Table 1 and selected bond lengths are listed in Table 2. Hydrogen bonds in the compounds **2**–**5** are given in Table 3. The topological analysis of the H-bonded networks in **2**–**5** was carried out taking into consideration only the conventional (strong) hydrogen bonds D–H···A, wherein H···A <2.50 Å, D···A <3.50 Å, ∠(D–H···A) >120°, D and A stand for donor and acceptor atoms.[17]

4. Results and discussion

4.1 Crystal structures

4.1.1 $[Ni(5\text{-}Fnic)_2(\mu_2\text{-}H_2O)_{0.5}]_n$ (1)

The crystal structure of **1** reveals that the compound crystallizes in the tetragonal space group *P*4/ncc and features an intricate 3D metal-organic framework. The asymmetric unit of **1** contains one crystallographically unique Ni(II) atom, two distinct μ_3-and μ_2-5-Fnic$^-$ ligands, and a half μ_2-H_2O moiety. As depicted in Fig. 1a, each six-coordinate Ni(II) atom adopts a distorted octahedral $\{ZnN_2O_4\}$ geometry formed by three carboxylate O atoms of three 5-Fnic$^-$ ligands, two N atoms of other two 5-Fnic$^-$ moieties, and one O atom of μ_2-H_2O group. The Ni–O bonds range from 2.043(2) to 2.100(2) Å, whereas the Ni–N distances vary from 2.089(2) to 2.109(2) Å, which are comparable to those found in other reported Ni(II) compounds.[9,18] In **1**, the 5-Fnic$^-$ moieties adopt two different coordination modes (Scheme 1, modes I and II), in which the carboxylate groups are either the η^1:η^0 monodentate or μ_2-η^1:η^1 bidentate. Two Ni(II) centers are bridged by carboxylate groups from two μ_3-5-Fnic$^-$ blocks and one μ_2-H_2O ligand, generating a dinickel(II) unit with the $[Ni_2(\mu\text{-}COO)_2(H_2O)]$ core (Fig. 1b) and Ni···Ni separation of 3.499(3) Å. Further linkage of these Ni_2 units via both the μ_2- and μ_3-5-Fnic$^-$ moieties furnishes a complex 3D metal-organic framework (Fig. 1c). To better understand the structure of this 3D MOF, we carried out its topological analysis using the concept of the simplified underlying net.[17] Such a net was generated (Fig. 1d) upon reducing the μ_2- and μ_3-5-Fnic$^-$ and μ_2-H_2O moieties to their centroids, thus resulting in a 3D framework assembled from the 6-connected Ni and 3-connected μ_3-5-Fnic$^-$ nodes, as well as the 2-connected μ_2-5-Fnic$^-$ and μ_2-H_2O

linkers. Topological analysis of this framework disclosed a binodal 3,6-connected net with a very rare **3,6T10** topology[17,19] and the point symbol of (3.4.5)($3^2.4^3.5.6^3.7^6$), wherein the (3.4.5) and ($3^2.4^3.5.6^3.7^6$) notations are those of the μ_3-5-Fnic$^-$ and Ni nodes, respectively. The rarity of the present topological type was corroborated by a search of various databases (CSD[15c], TOPOS,[17] and RCSR[19c]), revealing only a single example of the **3,6T10** framework.[20] Interestingly, it concerns a related nickel(II) coordination polymer derived from nicotinic acid, but its topological analysis and classification have not been performed in the original publication.[20] Hence, the present work also contributes to the topological identification of unusual metal-organic frameworks, which has been an important research direction in recent years.[17,19]

Scheme 1.

Fig. 1.

4.1.2 [Co(5-Fnic)$_2$(H$_2$biim)]$_n$ (2)

The asymmetric unit of compound **2** contains one crystallographically unique Co(II) atom, two distinct 5-Fnic$^-$ ligands, and one H$_2$biim moiety. As depicted in Fig. 2a, each six-coordinate Co(II) atom exhibits a distorted octahedral {CoN$_4$O$_2$} geometry formed by two carboxylate O atoms of one μ_2-5-Fnic$^-$ block, two N atoms of two different 5-Fnic$^-$ ligands, and two N atoms of one H$_2$biim moiety. The Co–O [2.174(2)–2.191(2) Å] and Co–N [2.086(2)–2.162(2) Å] bond lengths are in good agreement with those observed in some other Co(II) compounds.[8,9] In **2**, the 5-Fnic$^-$ ligands exhibit two different η^1- and μ_2-coordination modes (Scheme 1, modes III and

IV), in which the carboxylate group either shows a η^1:η^1 bidentate mode or remains uncoordinated. The H_2biim ligand acts in a bidentate chelating mode; the dihedral angle of two imidazole groups is 2.08º. The μ_2-5-Fnic$^-$ moieties alternately link the adjacent Co(II) centers to form a linear 1D metal-organic chain with the Co···Co separation of 7.820(3) Å (Fig. 2b). The neighboring chains are assembled into 2D supramolecular sheet motifs through strong N–H···O hydrogen bonds (Fig. 4c). These sheets are further held together via the π-π packing interactions (the centroid-centroid separation of adjacent imidazole planes of the H_2biim ligands is 3.719(2) Å) (Figs. S1 and S2). The above-mentioned 2D sheets formed via the conventional H-bonds[17a] were classified from the topological viewpoint, following the methodology developed for the topological analysis of H-bonded nets.[17,21] The topological analysis of an underlying network of **2** disclosed an interesting example of parallel 2D+2D interpenetration,[22] wherein each H-bonded layer is composed of 4-connected Co nodes and 2-connected 5-Fnic$^-$and H_2biim linkers (Fig. 2d), giving rise to a uninodal 4-connected net with the **sql** topology and the point symbol of $(4^4.6^2)$.

Fig. 2.

4.1.3 {[Cd(5-Fnic)$_2$(phen)]·2H$_2$O}$_n$ (3)

The compound **3** crystallizes in the monoclinic space group $P2_1/n$ and also features a linear 1D metal-organic chain structure. The asymmetric unit bears one crystallographically independent Cd(II) atom, one terminal 5-Fnic$^-$ and one μ_2-5-Fnic$^-$ block, one phen ligand, and two lattice water molecules. As depicted in Fig.

3a, the six-coordinate Cd(II) atom adopts a distorted octahedral {CdN_3O_3} geometry taken by three O atoms from the two distinct 5-Fnic$^-$ moieties and three N atoms from one 5-Fnic$^-$ and one phen ligand. The Cd–O and Co–N bond distances are in the 2.243(5)–2.437(5) and 2.313(7)–2.417(6) Å ranges, respectively. In **3**, the 5-Fnic$^-$ ligands show two different coordination modes (Scheme 1, modes III and V), in which the carboxylate groups are either η^1:η^0 monodentate or η^1:η^1 bidentate. It should be mentioned that the N atom of 5-Fnic$^-$ remains uncoordinated in the mode V. The μ_2-5-Fnic$^-$ moieties alternately bridge the adjacent Cd(II) centers to form a linear 1D metal-organic chain (Fig. 3b). The neighboring chains are sewed up into 1D double chain motifs though strong O–H···O hydrogen bonds involving crystallization water molecules (Fig. 3c). The resulting double chain motifs are further assembled into a 3D supramolecular framework via the weak C–H···π interactions (Fig. S3). After simplification procedure,[17a] the topological analysis of the above-mentioned double chain motifs revealed an underlying binodal 3,3-connected net with the unique topology defined by the point symbol of (5^2.8)(5^3), wherein the (5^2.8) and (5^3) notations correspond to the 3-connected Cd and 5-Fnic$^-$ nodes, respectively. An unprecedented character of this topological type was confirmed by a search of different databases.[15c,17,19c]

Fig. 3.

4.1.4 [Cd(5-Fnic)$_2$(H$_2$biim)$_2$] (4)

Compound **4** is a discrete 0D monomer. As shown in Fig. 4a, the six-coordinate Cd(II) center is bound by two carboxylate O atoms from two symmetry equivalent 5-Fnic$^-$

ligands and four N atoms from two symmetry equivalent H_2biim moieties, thus forming a distorted octahedral {CdN_4O_2} geometry. The Cd–O bonds are 2.450(2) Å, while the Cd–N distances vary from 2.292(3) to 2.303(2) Å; all these distances are comparable to those found in the reported Cd(II) compounds.[8,9,23] In **4**, the 5-Fnic$^-$ acts as a terminal ligand (Scheme 1, mode V), in which the carboxylate group is in the η^1:η^0 monodentate mode. The discrete monomeric units of **4** are interlinked by the strong N–H···O hydrogen bonds to form 1D chains, which are further assembled via the weak C–H···N interactions to generate 2D sheet motifs (Fig. 4b, Table 3). From the topological viewpoint, the 1D H-bonded chains in **4** can be classified as an underlying uninodal 2-connected **2C1** topological network composed of the [Cd(5-Fnic)$_2$(H_2biim)$_2$] molecular nodes (Fig. 4c).

Fig. 4.

4.1.5 [Co(5-Fnic)$_2$(H_2O)$_4$] (5)

Compound **5** also possesses a discrete monomeric structure. As represented in Fig. 5a, the six-coordinate Co(II) atom features a distorted octahedral {CoN_2O_4} geometry, filled by four symmetry equivalent O atoms of terminal H_2O ligands and two N atoms of the symmetry equivalent 5-Fnic$^-$ moieties. The Co–O [2.102(2) Å] and Co–N [2.157(3) Å] bonds are in good agreement with those distances observed in **2** and other related Co(II) compounds.[8,9] The 5-Fnic$^-$ blocks adopt the coordination mode V with the carboxylate groups remaining uncoordinated. The discrete monomeric units of **5** are interlinked by the repeating O–H···O hydrogen bonds to generate a symmetric 3D H-bonded framework (Fig. 5b and Table 3). From the topological perspective,[17,19]

this framework is composed of the $[Co(5\text{-Fnic})_2(H_2O)_4]$ molecular nodes and can be classified as an underlying uninodal 6-connected net (Fig. 5c) with the **pcu** (alpha-Po primitive cubic) topology and the point symbol of $(4^{12}.6^3)$.

4.1.6 Coordination modes of 5-fluoronicotinate blocks and structural comparison

As depicted in Scheme 1, the 5-Fnic$^-$ blocks in **1**–**5** behave as versatile N,O,O- (modes I, III), N,O- (mode II), N- (mode IV), or O-donors (type V), acting either as μ_2- and μ_3-brdiging or terminal ligands. In particular, the carboxylate group of 5-Fnic$^-$ can be in a $\eta^1{:}\eta^0$ monodentate (Scheme 1, modes II, V), $\eta^1{:}\eta^1$ bidentate (mode III), and μ_2-$\eta^1{:}\eta^1$ bidentate (mode I) fashion, or remains uncoordinated (mode IV). Hence, the structures of **1**–**5** vary from the 3D MOF (in **1**) to the linear 1D chains (in **2** and **3**) and the 0D discrete monomers (in **4** and **5**), which give rise to the topologically distinct metal-organic (in **1**) or H-bonded (in **2**–**5**) networks. The observed structural differences indicate that 5-fluoronicotinate moiety acts as a versatile building block for the construction of coordination compounds, the dimensionality, topology, and supramolecular features of which depend on the type of central metal ion and the presence (optional) of the N,N-ancillary ligand.

4.2 Thermal analysis

The thermal stability of compounds **1**–**5** was studied under nitrogen atmosphere by thermogravimetric analysis (TGA) and the obtained plots are given in Fig. 6. The compound **1** releases its half water ligand (exptl, 2.57%; calcd, 2.59%) in the

167–188 °C range, followed by the decomposition at 257 °C. The TGA curves of **2** and **4** indicate that these derivatives are stable up to 258 and 215°C, respectively, and then decompose upon further heating. Superior thermal stability of **2** can be explained by the 2D+2D interpenetration of the H-bonded layers in comparison with the non-interpenetrating 1D H-bonded chains in **4**. For **3**, the weight loss associated with the removal of two crystallization water molecules is observed in the 62–100 °C interval (exptl, 6.15%; calcd, 5.91%), and the decomposition of the remaining solid begins at 302 °C. For **5**, there are two distinct thermal effects in the 116–281 °C range that correspond to the removal of four coordinated H_2O molecules (exptl, 17.20%; calcd, 17.51%). Further heating up to 343 °C leads to the decomposition of a dehydrated sample. In general, the thermal behavior of compounds **1–5** is comparable to that of other related coordination compounds bearing nicotinate derivatives.[24]

Fig. 6.

4.3 Luminescent properties

The emission spectra of 5-fluoronicotinic acid (5-FnicH) and its cadmium(II) derivatives **3** and **4** were measured in the solid state at room temperature (Fig. 7). The uncoordinated 5-FnicH shows a weak photoluminescence with an emission maximum at 455 nm, if excited at 392 nm. In contrast, the compounds **3** and **4** display the significantly more intense emission bands with the maxima at 456 nm (λ_{ex} = 380 nm) and 535 nm (λ_{ex} = 450 nm), respectively. These bands can be due to the intraligand ($\pi^*\rightarrow n$ or $\pi^*\rightarrow\pi$) emission.[25] The enhancement of luminescence in the coordination

compounds can be associated with the type of ligand binding to metal centers,[25] and can also be influenced by the H-bonding interactions.[26,27] A somewhat stronger emission intensity in **3** over **4** can potentially be explained by their structural differences in terms of dimensionality, coordination modes of 5-Fnic$^-$ blocks, and presence of different N,N-donor ligands.

Fig. 7.

4.4 Magnetic properties

Variable-temperature magnetic susceptibility studies were carried out on powder samples of **1** and **2** in the 2–300 K temperature range. For the Ni(II) MOF **1**, the $\chi_M T$ value at 300 K is 1.12 cm^3·mol^{-1}·K, which is higher than the spin only value of 1.00 cm^3·mol^{-1}·K for one magnetically isolated Ni(II) center (S_{Ni} = 1, g = 2.0). Upon cooling, the $\chi_M T$ value drops down very slowly from 1.12 cm^3·mol^{-1}·K at 300 K to 1.08 cm^3·mol^{-1}·K at 22 K, and then decreases steeply to 0.50 cm^3·mol^{-1}·K at 2 K (Fig. 8). In the 50–300 K interval, the χ_M^{-1} *vs*. T plot for **1** obeys the Curie-Weiss law with a Weiss constant θ of –10.12 K and a Curie constant C of 1.11 cm^3·mol^{-1}·K, suggesting a weak antiferromagnetic interaction between the Ni(II) ions. Because of the long separation between the adjacent Ni_2 units, only the coupling interactions within the dinickel(II) blocks were considered.

We tried to fit the magnetic data of **1** using the following expression[28] for a dinuclear Ni(II) unit:

$$H = -JS_1S_2$$

$$\chi_{M'} = \frac{N\beta^2 g^2}{3k(T-\theta)} \frac{\sum S'(S'+1)(2S'+1)e^{-E(S')/kT}}{\sum (2S'+1)e^{-E(S')/kT}}$$

$$\chi_M = \chi_{M'}(1-\rho) + \frac{4S(S+1)N\beta^2 g^2 \rho}{3kT} + \text{TIP}$$

where ρ is a paramagnetic impurity fraction and TIP is temperature independent paramagnetism. Using this model, the susceptibility for **1** above 2.0 K was simulated, leading to the values of J = –2.21 cm^{-1}, g = 2.11, ρ = 0.011, and TIP = 378 × 10^{-6} cm^3 mol^{-1}, with the agreement factor R = 4.84 × 10^{-4} (R = $\sum(_{obs}T-_{calc}T)^2/\sum(_{obs}T)^2$). The negative J parameter confirms that a weak antiferromagnetic exchange coupling exists between the adjacent Ni(II) centers, which is in agreement with a negative θ value. In the structure of **1** (Fig. 1b), there are two types of the magnetic exchange pathways within the dinuclear units, namely via the μ_2-H$_2$O and μ_2-η^1:η^1-carboxylate (*syn-syn*) bridges. According to previous studies, the magnetic interaction is highly sensitive to the value of the Ni–O–Ni bridging angle, showing the domination of the Ni–Ni ferromagnetic coupling when the Ni–O–Ni angles are 90±14º.[29] The larger Ni–O–Ni angles in the Ni$_2$ unit [112.81(12)º] might suggest that the O bridges could be responsible for an antiferromagnetic exchange component. Meanwhile, the *syn-syn* carboxylate group bridging is likely to have a dominant antiferromagnetic effect. Hence, the small –J value observed for **1** (–2.21 cm^{-1}) could well be a result of two compatible exchange effects.

Fig. 8.

The temperature-dependent magnetic properties of **2** are shown in Fig. 9 in the

form of $\chi_M T$ *vs.* T curve. The $\chi_M T$ value of 2.76 $cm^3 \cdot mol^{-1} \cdot K$ at 300 K is much larger than the value (1.87 $cm^3 \cdot mol^{-1} \cdot K$) expected for one magnetically isolated high-spin Co(II) ion (S = 3/2, g = 2.0). This is a common phenomenon for Co(II) ions due to their strong spin-orbital coupling interactions.[8,9] The $\chi_M T$ values steadily decrease on lowering the temperature and reach the minimum of 1.48 $cm^3 \cdot mol^{-1} \cdot K$ at 1.99 K. Between 100 and 300 K, the magnetic susceptibility can be fitted to the Curie-Weiss law with C_M = 2.90 $cm^3 \cdot mol^{-1} \cdot K$ and θ = –14.7 K. These results indicate an antiferromagnetic interaction between the adjacent Co(II) ions.

We tried to fit the magnetic data of **2** using the following expression for a 1D Co(II) chain:[30]

$$\chi_{chain} = (Ng^2\beta^2/kT)[2.0 + 0.0194x + 0.777x^2][3.0 + 4.346x + 3.232x^2 + 5.834x^3]^{-1} \quad x = |J|/kT$$

Using this rough model, the susceptibility for **2** was simulated, leading to the values of J = –6.18 cm^{-1} and g = 2.36, and the agreement factor $R = 4.47 \times 10^{-5}$. The magnetic behavior of compound **2** is comparable to that of a related cobalt(II) nicotinate derivative.[24b]

Fig. 9.

5. Conclusions

In the present study, we applied 5-fluoronicotinic acid as a versatile but still unexplored building block in crystal engineering, resulting in the synthesis and structural characterization of five new coordination compounds **1**–**5**. Depending on the type of metal(II) ion (Ni, Co, Cd) and the presence of optional N,N-donor ancillary ligand, the obtained structures vary from the intricate 3D metal-organic framework **1** to 1D coordination polymers **2** and **3** or discrete 0D monomers **4** and **5**.

The structures of **2**–**5** are further extended [1D→2D (**2**), 1D→1D (**3**), 0D→1D (**4**), and 0D→3D (**5**)] into various H-bonded networks by means of conventional hydrogen bonds. These H-bonded nets in **2**–**5** along with the coordination network in **1** were topologically classified, revealing (i) a very rare **3,6T10** MOF topology in **1**, (ii) an interesting example of parallel 2D+2D interpenetration of the **sql** nets in **2**, (iii) a binodal 3,3-connected 1D network with undocumented topology in **3**, and (iv) the **2C1** and **pcu** (alpha-Po primitive cubic) topologies in **4** and **5**, respectively.

Besides, by reporting some advanced topological features (namely, very rare topology in **1**, interpenetrated topology in **2**, or even unprecedented topology in **3**), the current work also contributes to the classification, identification, and prediction of various topological motifs in compounds that form either coordination or H-bonded networks.[17,19,21,22] Although a vast number of topological types has been theoretically predicted or experimentally determined, the identification of novel topologies is a constantly growing research direction.[17] In many cases, certain types of properties of coordination compounds can be rationalized by applying the topological analysis methods.[19,21,22] For example, an enhanced thermal stability of derivative **2** over **4** can be explained by the observed 2D+2D interpenetration of the **sql** nets in **2**.

Apart from topological characteristics, some of the obtained compounds reveal advanced luminescent properties. In fact, the types of ancillary ligands in cadmium(II) derivatives **3** and **4** appear to affect not only their basic structural features, dimensionality, and H-bonding interactions, but also luminescent characteristics with the maxima of strong emission bands ranging from 456 to 535 nm in **3** and **4**,

respectively. These luminescence features suggest that such compounds can potentially be applied as photoactive materials.

In summary, the disclosed herein structural, H-bonding, and topological rarity of the compounds **1**–**5**, as well as their rather interesting advanced properties (e.g., luminescence of **3** and **4**) open up the exploration of 5-fluoronicotinic acid as a promising building block in crystal engineering of metal-organic and supramolecular networks.

Supporting information available

Additional structural fragments (Figures S1–S3) and X-ray crystallographic files in CIF format (CCDC 1030268–1030272 for **1**–**5**, respectively).

Acknowledgements

This work was financially supported by the National Natural Science Foundation of China (Project 21201091) and the Fundamental Research Funds for the Central Universities (Project lzujbky-2013-59). AMK acknowledges the Foundation for Science and Technology (FCT), Portugal (PTDC/QUI-QUI/121526/2010, PEst-OE/QUI/UI0100/2013).

References

1 (a) Y. Ma, A. L. Cheng, B. Tang and E. Q. Gao, *Dalton Trans.*, 2014, **43**, 13957–13964; (b) B. Xu, J. Li and N. N. Kong, C. C. Li, Inorg. *Chem. Commun.*,

2014, **47**, 119–122; (c) G. M. Zhuang, X. B. Li and E. Q. Gao, *Inorg. Chem. Commun.*, 2014, **47**, 134–137; (d) J. Z. Gu, D. Y. Lv, Z. Q. Gao, J. Z. Liu and W. Dou, *Transition Met. Chem.*, 2011, **36**, 53–58.

2 X. F. Zheng and L. G. Zhu, *J. Mol. Struct.*, 2013, **1039**, 1–7.

3 (a) L. Y. Yang, L. L. Xin, W. Gu, J. L. Tian, S. Y. Liao, P. Y. Du, Y. Z. Tong, Y. P. Zhang, R. Lv, J. Y. Wang and X. Liu, *J. Solid State Chem.*, 2014, **218**, 64–70;

(b) Y. X. Hu, Y. T. Qian, W. W. Zhang, Y. Z. Li and J. F. Bai, I*norg. Chem. Commun.*, 2014, **47**, 102–107;

(c) B. Van de Voorde, B. Bueken, J. Denayer and D. D. Vos, *Chem. Soc. Rev.*, 2014, **43**, 5766–5788.

4 (a) G. Akiyama, R. Matsuda, H. Sato and S. Kitagawa, *Chem. Asi. J.*, 2014, **9**, 2772–2777;

(b) L. Hashemi, A. Morsali, V. T. Yilmaz, O. Büyükgüngor, H. R. Khavasi, F. Ashouri and M. Bagherzadeh, *J. Mol. Struct.*, 2014, **1072**, 260–266;

(c) J. Gas, A. Corma, F. Kapteijn and F. X. L. Xamena, *ACS Catal.*, 2014, **4**, 361–378.

5 (a) Y. P. He, Y. X. Tan and J. Zhang, *Inorg. Chem.*, 2013, **52**, 12758–12762;

(b) X. Y. Duan, Q. Q. Meng, Y. Su, Y. Z. Li, C. Y. Duan, X. M. Ren and C. S. Lu, *Chem. Eur. J.*, 2011, **17**, 9936–9943.

6 (a) H. Wang, X. Y. Yang, Y. Q. Ma, W. B. Cui, Y. H. Li, W. G. Tian, S. Yao, Y. Gao, S. Dang and W. Zhu, *Inorg. Chim. Acta*, 2014, **416**, 63–68;

(b) F. A. L. Porta, P. H. Ramos, E. C. d Resende, M. C. Guerreiro, J. O. S. Giacoppo, T. C. Ramalho, J. R. Sambrano, J. Andrés and E. Longo, *Inorg. Chim. Acta*, 2014,

416, 200–206;

(c) W. G. Lu, L. Jiang, X. L. Feng and T. B. Lu, *Inorg. Chem.*, 2009, **48**, 6997–6999.

7 W. G. Lu, C. Y. Su, T. B. Lu, L. Jiang and J. M. Chen, *J. Am. Chem. Soc.*, 2006, **128**, 34–35.

8 J. Z. Gu, Z. Q. Gao and Y. Tang, *Cryst. Growth Des.*, 2012,**12**, 3312−3323.

9 J. Z. Gu, A. M. Kirillov, J. Wu, D. Y. Lv, Y. Tang and J. C. Wu, *CrystEngComm.*, 2013, **15**, 10287−10303.

10 T. Liu, S. N. Wang, J. Lu, J. M. Dou, D. C. Li and J. F. Bai, *CrystEngComm.*, 2013, **15**, 5476–5489.

11 L. Chen, S. H. Gou and J. Q. Wang, *J. Mol. Struct.*, 2011, **991**, 149–157.

12 J. Z. Gu, D. Y. Lv, Z. Q. Gao, J. Z. Liu, W. Dou and Y. Tang, *J. Solid State Chem.*, 2011,**184**, 675−683.

13 Y. Zhang, B. B. Guo, S. F. Liu and G.. Li, *Cryst. Growth Des.*, 2013, **13**, 367−376.

14 (a) B.B. Ding, Y. Q. Weng, Z. W. Mao, C. K. Lan, X. M. Chen and B. H. Ye, *Inorg. Chem.*, 2005, **44**, 8836–8845;

(b) L. Chen, S. H. Gou and J. Q. Wang, *J. Mol. Struct.*, 2011, **991**, 149–157;

15 (a) C. P. Li, J. Chen, P. W. Liu and M. Du, *CrystEngComm*, 2013, **15**, 9713–9721.

(b) X.-M. Wang, W. P. Wu, Y. H. Jiang, G. P. Yang and Z. P. Xi, *Chin. J. Inorg. Chem*., 2014, **30**, 192–203.

(c) See the Cambridge Structural Database (CSD, version 5.35, May 2014): F. H. Allen, *Acta Crystallogr.* 2002, **B58**, 380–388.

16 (a) G. M. Sheldrick, *Acta Crystallogr.*, 1990, **A 46**, 467–473;

(b) G. M. Sheldrick, SHELXS-97*, A Program for X-ray Crystal Structure Solution*,

and SHELXL-97, A Program for X-ray Structure Refinement, Göttingen University, Germany, 1997.

17 (a) V. A. Blatov, *IUCr CompComm Newsletter*, 2006, **7**, 4–38;

(b) V. A. Blatov, A. P. Shevchenko and D. M. Proserpio, *Cryst. Growth Des.*, 2014, **14**, 3576–3586.

18 D. Y. Lv, Z. Q. Gao, J. Z. Gu, R. Ren and W. Dou, *Transition Met. Chem.*, 2011, **36**, 313–318.

19 (a) M. O'Keeffe, O. M. Yaghi, *Chem. Rev.*, 2012, **112**, 675–702.

(b) M. Li, D. Li, M. O'Keeffe and O. M. Yaghi, *Chem. Rev.*, 2014, **114**, 1343−1370.

(c) The Reticular Chemistry Structure Resource (RCSR) Database; M. O'Keeffe, M. A. Peskov, S. J. Ramsden and O. M. Yaghi, *Acc. Chem. Res.* 2008, **30**, 1782–1789.

20 P. Ayyappan, O. R. Evans and W. Lin, *Inorg. Chem.* 2001, **40**, 4627–4632.

21 P. N. Zolotarev, M. N. Arshad, A. M. Asiri, Z. M. Al-amshany and V. A. Blatov, *Cryst. Growth Des.,* 2014, **14**, 1938–1949.

22 L. Carlucci, G. Ciani, D. M. Proserpio, T. G. Mitina and V. A. Blatov, *Chem. Rev.*, 2014, **114**, 7557–7580.

23 D. Sun, L. L. Han, S. Yuan, Y. K. Deng, M. Z. Xu and D. F. Sun, *Cryst. Growth Des.*, 2013, **13**, 377−385.

24 (a) J. Z. Gu, J. Wu, A. M. Kirillov, D. Y. Lv, Y. Tang and J. C. Wu, *J. Solid State Chem.*, 2014, 2**13**, 256−267. (b) H. J. Li, Z. Q. Gao and J. Z. Gu, *Chin. J. Struct. Chem.,* 2014, **33**, 1713–1721.

25 Y. Zhang, B. B. Guo, L. Li, S. F. Liu and G. Li, *Cryst. Growth Des.*, 2013, **13**,

367−376.

26 Q. Wang, X. H. Yan, H. R. Zhang, W. S. Liu, Y. Tang and M. Y. Tan, *J. Solid State Chem.*, 2011, **184**, 164−170.

27 Y. L. Guo, W. Dou, X. Y. Zhou, W. S. Liu, W. W. Qin, Z. P. Zang, H. R. Zhang and D. Q. Wang, *Inorg. Chem.*, 2009, **48**, 3581−3590.

28 L. K. Thompson, V. Niel, H. Grove, D. O. Miller, M. J. Newlands, P. H. Bird, W. A. Wickramasinghe and A. B. P. Lever, *Polyhedron*, 2004, **23**, 1175−1184.

29 P. Mahata, S. Natarajan, P. Panissod and M. Drillon, *J. Am. Chem. Soc.*, 2009, **131** 10140−10150.

30 O. Kahn, *Molecular Magnetism*; VCH Publishers Inc.: New York, 1993; p 258.

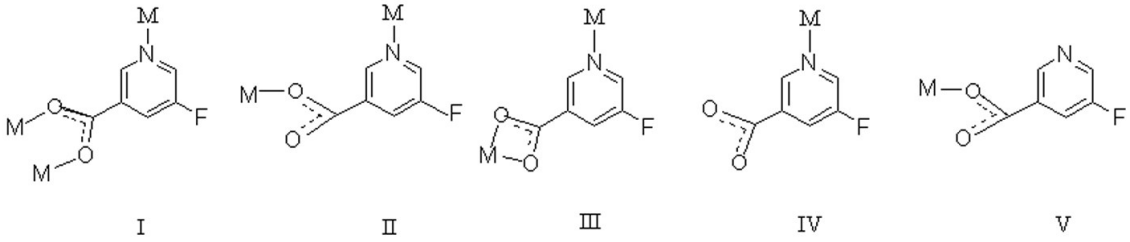

Scheme 1. Various coordination modes of 5-Fnic$^-$ in compounds **1**–**5**.

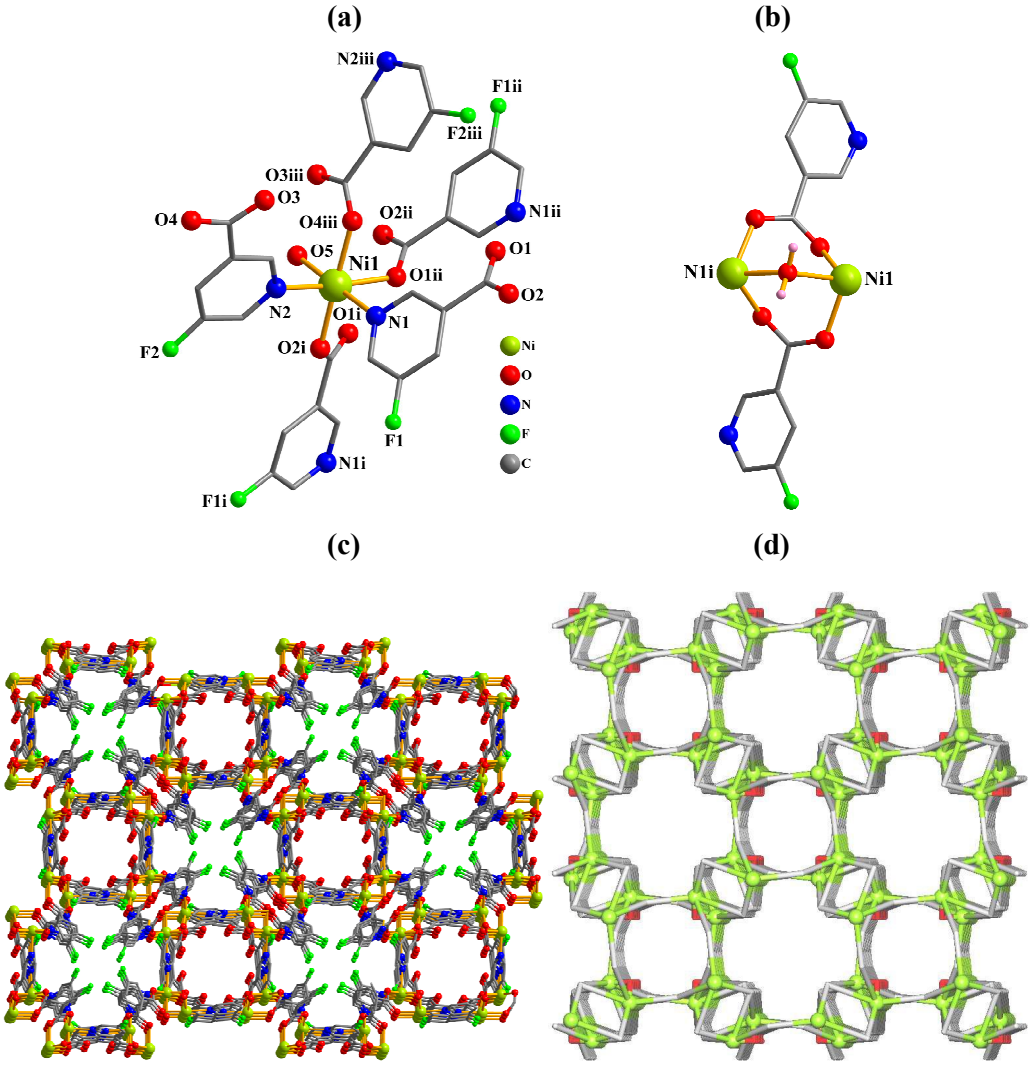

Fig. **1.** Structural fragments of **1**. (a) Coordination environment of the Ni(II) atom. (b) Dinickel unit. (c) Perspective of the 3D MOF along the *ab* plane. (d) Topological representation of the underlying binodal 3,6-connected 3D framework with the **3,6T10** topology (view along the *c* axis). Further details: (a) symmetry codes: i = *y*, *x*, *z* – 1/2; ii = –*x* + 1, –*y* + 1, –*z* + 1; iii = –*y* + 1, *x* + 1/2, –*z* + 1; (b) symmetry code: i = –*x* + 1, –*y* + 1, –*z* + ½; (a–c) H atoms (apart from those of H_2O) are omitted for clarity; (d) color codes: 6-connected Ni nodes (pale green), centroids of 3-connected 5-Fnic$^-$ nodes (gray), centroids of 2-connected μ-H_2O linkers (red).

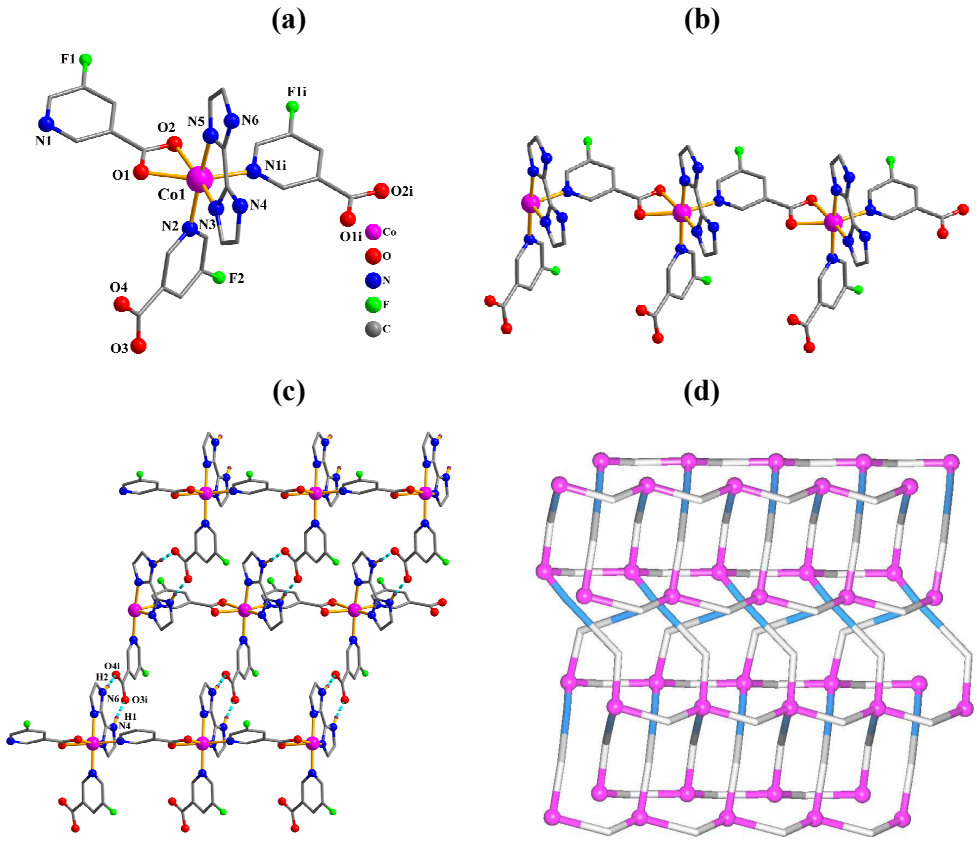

Fig. **2**. Structural fragments of **2**. (a) Coordination environment of the Co(II) atom. (b) Perspective of the 1D metal-organic chain along the *ab* plane. (c) 2D H-bonded sheet motif along the *ab* plane (blue dashed lines represent the H-bonds). (d) Topological representation (view along the *c* axis) of two underlying 2D H-bonded layers showing their parallel 2D+2D interpenetration; each layer is a uninodal 4-connected net with the **sql** topology. Further details: (a) symmetry code: i = *x*–1, *y*, *z*; (c) symmetry code: i = *x* – 1/2, *y* + 1/2, –*z* + ½; (a–c) H atoms (apart from those participating in H-bonds) are omitted for clarity; (d) color codes: 4-connected Co nodes (magenta), centroids of 2-connected 5-Fnic^{-} (gray) and H_2biim (blue) linkers.

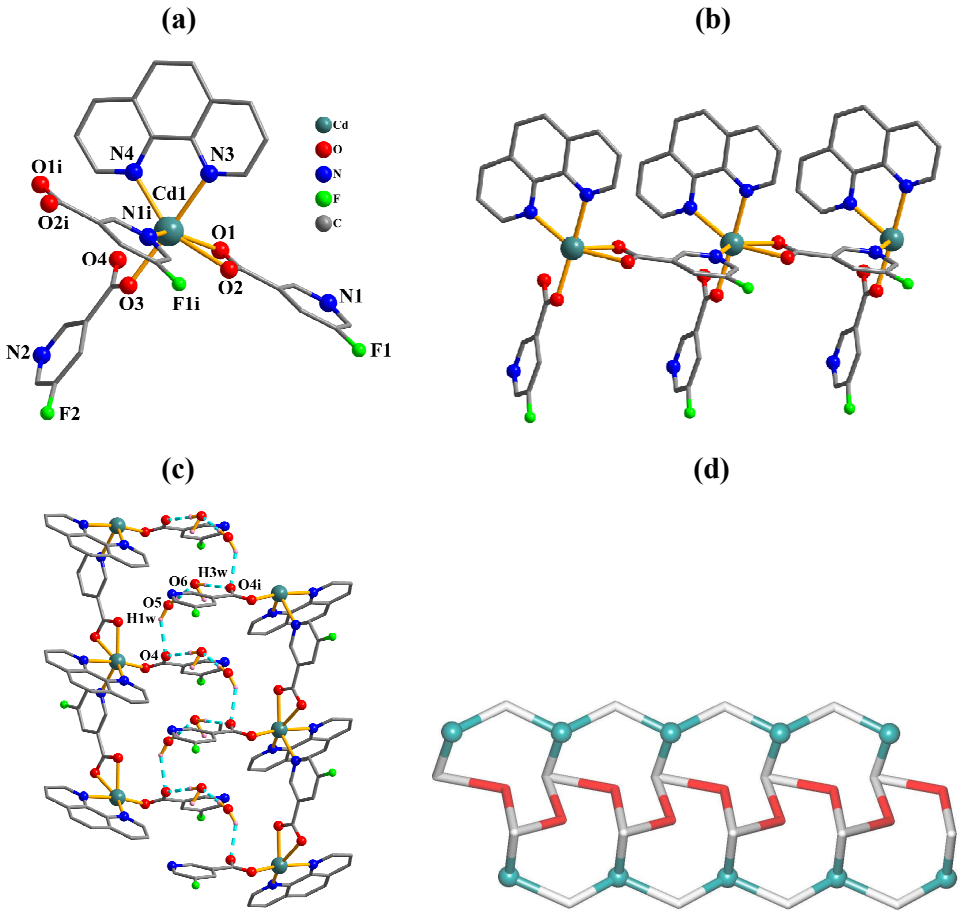

Fig. 3. Structural fragments of **3**. (a) Coordination environment of the Cd(II) atom. (b) Linear 1D metal-organic chain. (c) Perspective of a double chain along the *bc* plane (blue lines present the H-bonding). (d) Topological representation (view along the *a* axis) of an underlying 1D H-bonded double chain classified as a binodal 3,3-connected net with the unique topology. Further details: (a) symmetry code: i = *x*, *y* + 1, *z*; (c) symmetry code: i = –*x* + 1/2, *y* – 1/2, –*z* + 1/2; (a–c) H atoms (apart from those participating in H-bonds) are omitted for clarity; (d) color codes: 3-connected Cd nodes (turquoise), centroids of 3-connected 5-Fnic^{-} nodes (gray) and centroids of 2-connected $(H_2O)_2$ linkers (red).

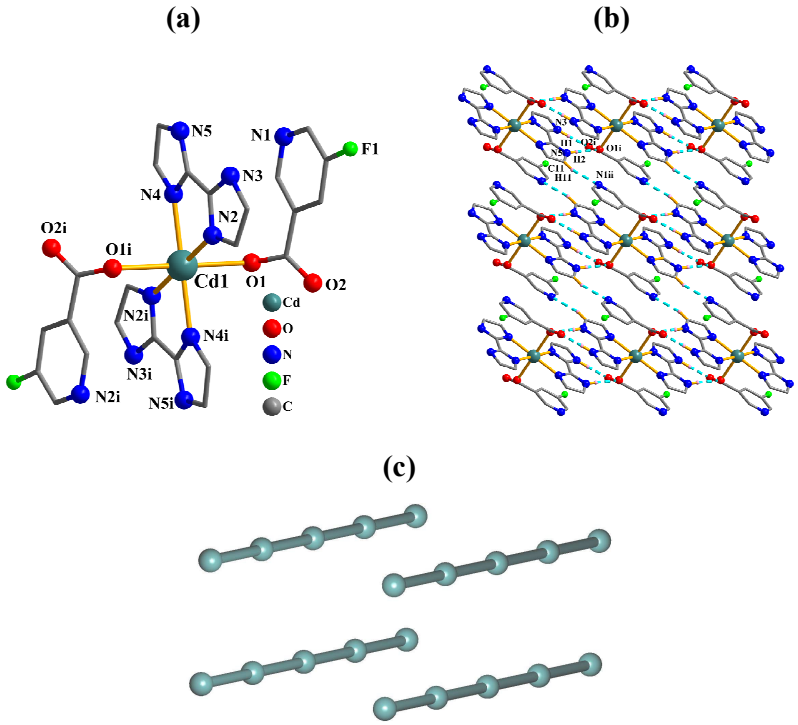

Fig. 4. Structural fragments of **4**. (a) Coordination environment of the Cd(II) atom. (b) Arrangement of mononuclear blocks into a 2D sheet motif via strong and weak H-bonding interactions (blue dashed lines represent the H-bonds; view along the *ab* plane). (c) Topological representation of the 1D chains formed via strong H-bonds, showing an underlying uninodal 2-connected network with the 2C1 topology. Further details: (a) symmetry code: i = –*x* + 2, –*y* + 1, –*z* + 1; (b) symmetry codes: i = *x* – 1, *y*, *z*; ii = –*x* + 1, –*y* + 2, –*z*; (a, b) H atoms (apart from those participating in H-bonds) are omitted for clarity; (c) centroids of 2-connected $[Cd(5\text{-Fnic})_2(H_2biim)_2]$ molecular nodes (turquoise).

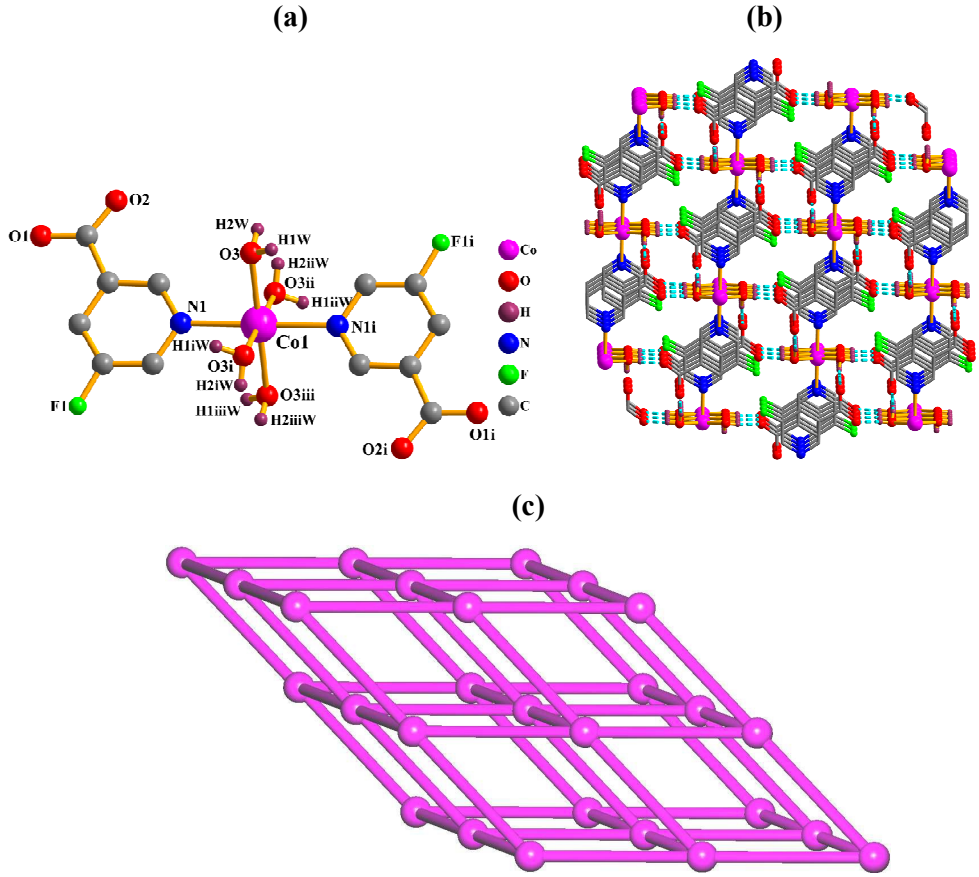

Fig. **5**. Structural fragments of **5**. (a) Coordination environment of the Co(II) atom. (b) Perspective of the 3D H-bonded framework along the *ac* plane (blue dashed lines represent the H-bonds). (c) Topological representation (view along the *a* axis) of the underlying uninodal 6-connected 3D H-bonded framework with the **pcu** topology. Further details: (a) Symmetry codes: i = –*x* + 1, –*y* + 1, –*z* + 1; ii = *x*, –*y* + 1, *z*; iii = –*x* + 1, *y*, –*z* + 1; (a, b) H atoms (apart from those participating in H-bonds) are omitted for clarity; (c) centroids of 6-connected $[Co(5\text{-}Fnic)_2(H_2O)_4]$ molecular nodes (magenta).

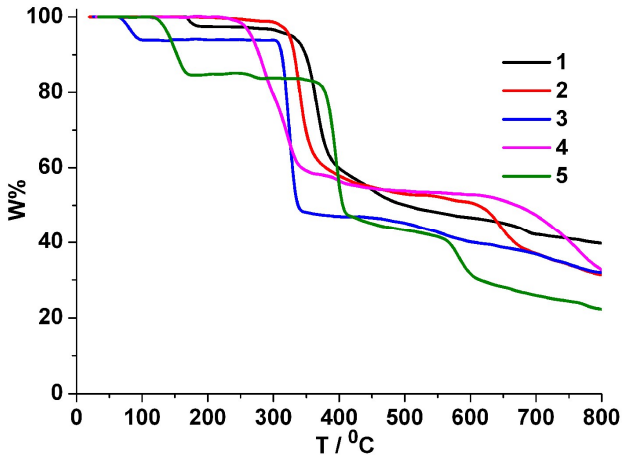

Fig. **6**. Thermogravimetric analysis (TGA) curves of compounds **1**–**5**.

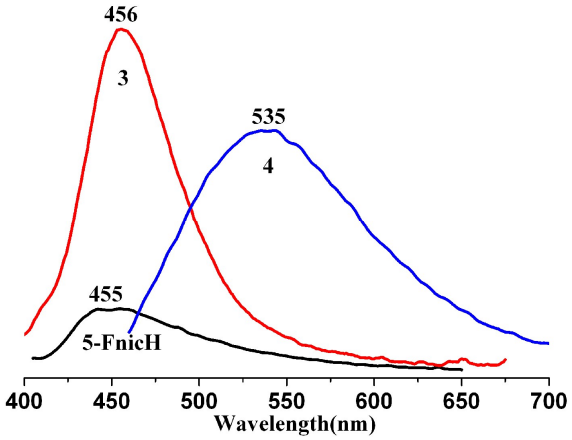

Fig. **7**. Solid state emission spectra of 5-FnicH, **3** and **4** (λ_{ex} of 392, 380 and 450 nm, respectively).

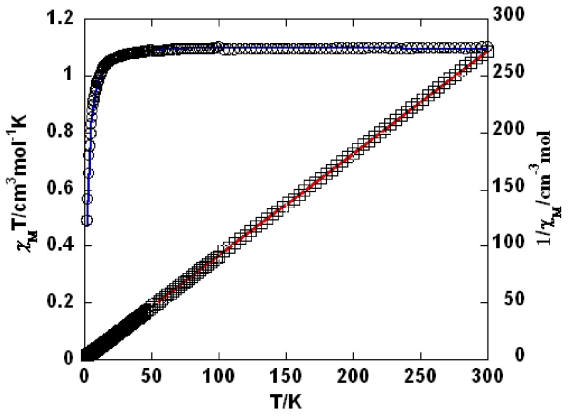

Fig. **8**. Temperature dependence of $\chi_M T$ (O) and $1/\chi_M$(□) vs. T for compound **1**. The blue line represents the best fit to the equations in the text. The red line shows the Curie-Weiss fitting.

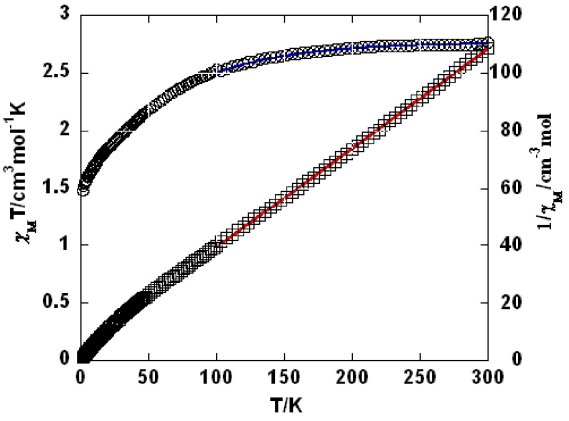

Fig. **9**. Temperature dependence of $\chi_M T$ (O) and $1/\chi_M$(□) vs. T for compound **2**. The blue line represents the best fit to the equations in the text. The red line shows the Curie-Weiss fitting.

Table 1. Crystallographic data for **1**–**5**.

Complex	**1**	**2**	**3**	**4**	**5**
Chemical formula	$C_{12}H_7F_2NiN_2O_{4.5}$	$C_{18}H_{12}F_2CoN_6O_4$	$C_{24}H_{18}F_2CdN_4O_6$	$C_{24}H_{18}F_2CdN_{10}O_4$	$C_{12}H_{14}F_2CoN_2O_8$
Formula weight	347.91	473.27	608.82	660.88	411.18
Crystal system	Tetragonal	Orthorhombic	Monoclinic	Triclinic	Monoclinic
Space group	*P*4/*ncc*	*P*bcn	$P2_1/n$	*P*-1	*I*2/*m*
a/Å	20.5004(7)	7.8197(4)	14.6749(10)	7.3743(4)	8.4112(5)
b/Å	20.5004(7)	17.8112(9)	8.0043(4)	8.4333(5)	6.8339(5)
c/Å	13.9201(6)	26.5942(14)	21.4102(17)	10.3961(5)	13.2136(8)
α/°	90	90	90	92.632(2)	90
β/°	90	90	107.405(7)	94.015(2)	96.514(6)
γ/°	90	90	90	94.544(2)	90
V/Å^3	5850.2(4)	3704.0(3)	2399.8(3)	642.05(6)	754.63(9)
T/K	293(2)	296(2)	293(2)	293(2)	293(2)
Z	16	8	4	1	2
D_c/g cm^{-3}	1.580	1.697	1.685	1.709	1.810
μ/mm^{-1}	1.368	0.988	0.974	0.918	1.208
F(000)	2800	1912	1216	330	418
Refl. measured	14382	17808	9817	3262	1376
Unique refl. (R_{int})	2611 (0.0581)	3307 (0.0329)	4250(0.0682)	2243 (0.0186)	722 (0.0409)
GOF on F^2	1.041	1.025	1.058	1.062	1.002
R_1 $[I > 2\sigma(I)]^a$	0.0352	0.0278	0.0613	0.0240	0.0379
wR_2 $[I > 2\sigma(I)]^b$	0.0891	0.0649	0.1333	0.0622	0.0962

Table 2. Selected bond lengths [Å] and angles [°] for **1**–**5**.[a]

1					
Ni(1)-O(1)#2	2.075(2)	Ni(1)-O(2)#1	2.0429(19)	Ni(1)-O(4)#3	2.0800(19)
Ni(1)-O(5)	2.1001(15)	Ni(1)-N(1)	2.089(2)	Ni(1)-N(2)	2.109(2)
O(2)#1-Ni(1)-O(1)#2	95.54(7)	O(2)#1-Ni(1)-O(4)#3	178.05(8)	O(1)#2-Ni(1)-O(4)#3	82.53(8)
O(2)#1-Ni(1)-N(1)	90.31(8)	O(1)#2-Ni(1)-N(1)	85.61(8)	O(4)#3-Ni(1)-N(1)	89.81(8)
O(2)#1-Ni(1)-O(5)	88.65(6)	O(1)#2-Ni(1)-O(5)	91.36(7)	O(4)#3-Ni(1)-O(5)	91.13(6)
N(1)-Ni(1)-O(5)	176.69(9)	O(2)#1-Ni(1)-N(2)	90.89(8)	O(1)#2-Ni(1)-N(2)	173.20(8)
O(4)#3-Ni(1)-N(2)	91.05(9)	N(1)-Ni(1)-N(2)	92.16(9)	O(5)-Ni(1)-N(2)	90.99(9)
Ni(1)-O(5)-Ni(1)#5	112.81(12)				
2					
Co(1)-O(1)	2.1740(14)	Co(1)-O(2)	2.1907(14)	Co(1)-N(1)#1	2.1620(16)
Co(1)-N(2)	2.1363(17)	Co(1)-N(3)	2.0863(16)	Co(1)-N(5)	2.1271(18)
N(3)-Co(1)-N(5)	79.79(7)	N(3)-Co(1)-N(2)	90.92(6)	N(5)-Co(1)-N(2)	170.58(6)
N(3)-Co(1)-N(1)#1	97.22(6)	N(5)-Co(1)-N(1)#1	88.36(6)	N(2)-Co(1)-N(1)#1	94.33(6)
N(3)-Co(1)-O(1)	110.72(6)	N(5)-Co(1)-O(1)	95.64(6)	N(2)-Co(1)-O(1)	86.20(6)
N(1)#1-Co(1)-O(1)	152.05(6)	N(3)-Co(1)-O(2)	168.56(6)	N(5)-Co(1)-O(2)	93.76(6)
N(2)-Co(1)-O(2)	95.16(6)	N(1)#1-Co(1)-O(2)	91.99(5)	O(1)-Co(1)-O(2)	60.19(5)
3					
Cd(1)-O(1)	2.335(5)	Cd(1)-O(2)	2.437(5)	Cd(1)-O(3)	2.243(5)
Cd(1)-N(1)#1	2.364(5)	Cd(1)-N(3)	2.417(6)	Cd(1)-N(4)	2.313(7)
O(3)-Cd(1)-N(4)	111.4(3)	O(3)-Cd(1)-O(1)	99.2(2)	N(4)-Cd(1)-O(1)	118.2(2)
O(3)-Cd(1)-N(1)#1	81.3(2)	N(4)-Cd(1)-N(1)#1	96.1(2)	O(1)-Cd(1)-N(1)#1	142.09(19)
O(3)-Cd(1)-N(3)	169.2(2)	N(4)-Cd(1)-N(3)	70.1(3)	O(1)-Cd(1)-N(3)	89.01(19)
N(1)#1-Cd(1)-N(3)	88.0(2)	O(3)-Cd(1)-O(2)	95.0(2)	N(4)-Cd(1)-O(2)	153.6(2)
O(1)-Cd(1)-O(2)	54.89(17)	N(1)#1-Cd(1)-O(2)	87.22(18)	N(3)-Cd(1)-O(2)	83.9(2)
4					
Cd(1)-O(1)	2.4503(16)	Cd(1)-O(1)#1	2.4503(16)	Cd(1)-N(2)	2.3031(18)
Cd(1)-N(2)#1	2.3031(18)	Cd(1)-N(4)	2.2915(18)	Cd(1)-N(4)#1	2.2915(18)
N(4)-Cd(1)-N(4)#1	180.0	N(4)-Cd(1)-N(2)	75.02(6)	N(4)#1-Cd(1)-N(2)	104.98(6)
N(4)-Cd(1)-N(2)#1	104.98(6)	N(4)#1-Cd(1)-N(2)#1	75.02(6)	N(2)-Cd(1)-N(2)#1	180.0
N(4)-Cd(1)-O(1)#1	89.29(6)	N(4)#1-Cd(1)-O(1)#1	90.71(6)	N(2)-Cd(1)-O(1)#1	91.44(6)
N(2)#1-Cd(1)-O(1)#1	88.56(6)	N(4)-Cd(1)-O(1)	90.71(6)	N(4)#1-Cd(1)-O(1)	89.29(6)
N(2)-Cd(1)-O(1)	88.56(6)	N(2)#1-Cd(1)-O(1)	91.44(6)	O(1)#1-Cd(1)-O(1)	180.0
5					
Co(1)-O(3)	2.102(2)	Co(1)-O(3)#1	2.102(2)	Co(1)-O(3)#2	2.102(2)
Co(1)-O(3)#3	2.102(2)	Co(1)-N(1)	2.157(3)	Co(1)-N(1)#1	2.157(3)
O(3)-Co(1)-O(3)#1	180.0	O(3)-Co(1)-O(3)#2	90.86(14)	O(3)#1-Co(1)-O(3)#2	89.14(14)
O(3)-Co(1)-O(3)#3	89.14(14)	O(3)#1-Co(1)-O(3)#3	90.86(14)	O(3)#2-Co(1)-O(3)#3	180.00(11)
O(3)-Co(1)-N(1)#1	91.18(8)	O(3)#1-Co(1)-N(1)#1	88.82(8)	O(3)#2-Co(1)-N(1)#1	91.18(8)
O(3)#3-Co(1)-N(1)#1	88.82(8)	O(3)-Co(1)-N(1)	88.82(8)	O(3)#1-Co(1)-N(1)	91.18(8)
O(3)#2-Co(1)-N(1)	88.82(8)	O(3)#3-Co(1)-N(1)	91.18(8)	N(1)#1-Co(1)-N(1)	180.0

[a] Symmetry transformations used to generate equivalent atoms: #1 *y*, *x*, *z*–1/2; #2 –*x*+1, –*y*+1, –*z* +1; #3 –*y*+1, *x*+1/2, –*z*+1; #4 *y*, *x*, *z*+1/2; #5 –*y*+1, –*x*+1, –*z*+1/2 for **1**; #1 *x*–1, *y*, *z* for **2**; #1 *x*, *y*+1, *z* for **3**; #1 –*x*+21, –*y*+1, –*z* for **4**; #1 –*x*+1, –*y*+1, –*z*+1; #2 *x*, –*y*+1, *z* ; #3 –*x*+1, *y*, –*z*+1 for **5**.

Table 3. Conventional hydrogen bonds in crystal packing [Å, °] of **2**–**5**.

Complexes	D-H…A	*d*(D-H)	*d*(H…A)	*d*(D…A)	∠DHA	Symmetry code
2	N(6)-H(2)···O(4)	0.97	1.71	2.673	176	*x*-1/2, *y*+1/2, -*z*+1/2
	N(4)-H(1)···O(3)	0.87	1.75	2.623	173	*x*-1/2, *y*+1/2, -*z*+1/2
3	O(6)-H(3W) ···O(4)	0.85	1.98	2.84	178.0	-*x*+/2, *y*-1/2, -*z*+1/2
	O(5)-H(2W)···O(6)	0.85	1.75	2.60	177.8	
	O(5)-H(1W)···O(4)	0.99	2.19	3.04	142.9	
4	N(3)-H(1)···O(2)	0.92	1.83	2.743	170	*x*-1, *y*, *z*
	N(5)-H(2)···O(1)	0.85	1.87	2.709	173	*x*-1, *y*, *z*
5	O(3)-H(1W)···O(1)	0.82	1.94	2.742	164.8	*x*-1/2, *y*+1/2, *z*+1/2
	O(3)-H(2W)···O(2)	0.79	1.99	2.728	155	-*x*+2, -*y*+1, -*z*+1

Exploring 5-fluoronicotinic acid as a versatile building block for the generation of topologically diverse metal-organic and supramolecular Ni, Co, and Cd networks

Yan-Hui Cui, Jiang Wu, Alexander M. Kirillov, Jin-Zhong Gu* and Wei Dou

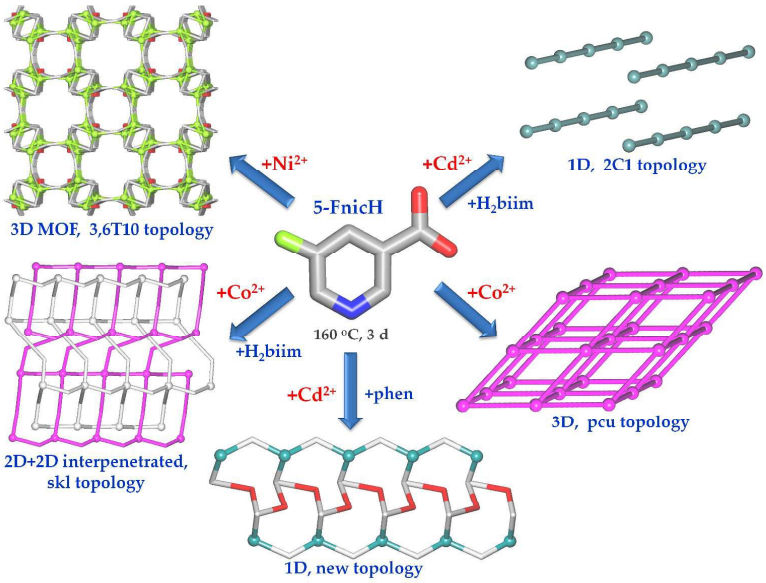

Five new coordination compounds driven by 5-fluoronicotinic acid were self-assembled and structurally characterized, revealing metal-organic or H-bonded networks with distinct topologies, including their rare or unreported examples.